Digital nuclear morphometry correlates to BAP-1 expression, gene expression class and metastasis-free survival in uveal melanoma

Christina Herrspiegel[1,2], Thonnie Rose O. See[3], Pia R. Mendoza[4], Hans E. Grossniklaus[3], and Gustav Stålhammar*[1,2]

[1]St. Erik Eye Hospital, Stockholm, Sweden

[2]Department of Clinical Neuroscience, Karolinska Institutet, Stockholm, Sweden, and

[3]Departments of Ophthalmology and Pathology, Emory University School of Medicine, Atlanta, Georgia, USA.

[4]Department of Pathology and Laboratory Medicine, Emory University School of Medicine, Atlanta, Georgia, USA.

*Corresponding author

Gustav Stålhammar, M.D. Ph.D. FEBO

Oncology and Pathology service, St. Erik Eye Hospital

Department of Clinical Neuroscience, Karolinska Institutet

Polhemsgatan 50, 112 82

Stockholm, Sweden

Email: gustav.stalhammar@ki.se

Phone: +46 8 672 30 00

ABSTRACT

Cytologic features such as the shape and size of tumor cells can predict metastatic death in uveal melanoma, but suffer from poor reproducibility. In this study, we investigate the interobserver concordance of digital morphometry, and correlate the results with established prognostic markers. The average number of cells analyzed in each of 27 tumors, was 1957 (SD 349). Mean time consumption was less than 2.5 minutes per tumor. Identical morphometric classification was obtained for ≥ 85 % of tumors in all twelve evaluated morphometric variables (κ 0.70–0.93). The mean nucleus area, nucleus perimeter, nucleus max caliper and nucleus to cell area ratio were significantly greater in tumors with low nuclear BRCA associated protein-1 expression (nBAP-1) and gene expression class 2. Patients had significantly shorter metastasis-free survival if their tumors had low nBAP-1 expression (Log-Rank p=0.002), gene expression class 2 (Log-Rank p=0.004) or tumor cell nuclei with long max calipers (Log-Rank p=0.004) as defined in a training cohort and then tested in a validation cohort. We conclude that digital morphometry can be fast and highly reproducible, that for the first time, morphometry parameters can be objectively quantitated in thousands of cells at a time, and that variables describing the shape and size of the nuclei correlate to nBAP-1 expression, gene expression class and prognosis in uveal melanoma.

1. Introduction

Uveal melanoma is the most common primary intraocular malignancy in adults (Singh et al., 2014). Less than 5 % of patients have clinically detectable metastases at the time of diagnosis (Singh et al., 2014). At a later stage however, up to 45 % of patients will develop metastases even if the eye containing the tumor has been removed (Kujala et al., 2003). Once macrometastases develop, there is no effective treatment and median patient survival is only 4-12 months (Augsburger et al., 2009; Carvajal et al., 2016).

Several methods for prognostication are in clinical use. Tumor thickness, diameter, location in the eye and presence of distant metastases determine tumor stage (Arnljots et al., 2018; Kivelä et al., 2017). Loss of chromosome 3 has a high positive and negative predictive value for metastasis (Bornfeld et al., 1996). Commercial gene tests based on the expression of 12 classifier genes have been developed and show excellent prognostic utility in separation of class 1 tumors with low metastatic risk from class 2 tumors with high metastatic risk (Onken et al., 2012). Furthermore, we have previously shown the prognostic utility of manual (Szalai et al., 2018) and digital image analysis-based (Stålhammar et al., 2019) determination of the level of nBAP-1.

In 1931, Callender described six types of uveal melanoma based on cytologic features such as cell shape and the size of the nucleus (Callender, 1931). The original classification could accurately predict metastatic death, but suffered from substantial intra- and interobserver discordance (Coleman et al., 1996; Gamel et al., 1992). After several modifications, the morphological classification of uveal melanoma now rely on assessments of the proportion of epitheloid tumor cells (McLean et al., 1983;

Seddon et al., 1987). Examination of cytological features still require a high level of cytologic expertise and suffer from poor reproducibility (Gamel et al., 1992). Computer-assisted methods have therefore been proposed as a way of facilitating these assessments. In 1982, Gamel *et al*. found that 13 of 18 nuclear and nucleolar features correlated significantly with patient mortality when evaluated with a digitizer superimposed on microscopic images at a rate of 100 cells per hour (Gamel et al., 1982). Since then, computers have improved manyfold in terms of their computing power, cost and the number and scope of software applications and we can now analyze a dozen of variables or more in thousands of cells per minute on inexpensive off-the-shelf laptop computers (Stålhammar et al., 2016; Stålhammar et al., 2018).

Consequently, we see an opportunity to analyze cell morphometry features with digital image analysis and compare these to other prognostic factors including nBAP-1 expression in uveal melanoma patients from one American and one European referral center.

2. Methods

2.1. Patients and Samples

The study adhered to the tenets of the Declaration of Helsinki. Methods were carried out in accordance with the relevant guidelines and regulations. The protocol for collection of specimens and data from St. Erik Eye Hospital, Stockholm, Sweden was approved by the regional ethical review board in Stockholm, and the protocol for collection of specimens and data from Emory Eye Center, Atlanta, GA, USA by the Emory Institutional Review Board.

87 Patients were identified in the archives of the Oncology and Pathology
88 service, St. Erik Eye Hospital and L.F. Montgomery Ophthalmic Pathology
89 Laboratory, Emory Eye Center. Inclusion criteria were: 1) Enucleation performed
90 before December 2017, 2) Histologically proven uveal melanoma, 3) paraffin block
91 available, 4) gene expression classification available, 5) clinicopathological data
92 available, including tumor thickness, diameter, location, T-category and cell type, 6)
93 follow-up data available, 7) sufficient tissue for BAP-1 immunohistochemistry.
94 Exclusion criteria were: 1) Prior history of plaque brachytherapy, proton beam
95 irradiation and/or transpupillary thermotherapy, and 3) tumor fully necrotic or fully
96 hemorrhagic. 27 patients met the criteria. Our follow-up data was confirmed and
97 further extended in telephone interviews with patients or relatives. Informed consent
98 was obtained from all participants.
99 In order to establish optimized morphometry thresholds for the distinction of
100 metastatic versus non-metastatic disease we divided our 27 patients into one training
101 and one validation cohort. When determining the relative size of the training and
102 validation cohorts, we considered previous research indicating that the ratio should be
103 inversely proportional to the square root of the number of free adjustable parameters
104 (Guyon, 1997). As we only evaluated one morphometric variable at a time, we set the
105 ratio to 1:1. 13 patients were randomized to the training cohort and 14 to the
106 validation cohort.
107
108 *2.2. Immunohistochemistry*
109 The paraffin blocks were cut into 4 μm sections, pretreated in EDTA-buffer at pH 9.0
110 for 20 minutes and incubated with mouse monoclonal antibodies against BAP-1

111 (clone C-4, Santa Cruz Biotechnology, Dallas, Texas, USA) and a red chromogen,
112 and finally counterstained with haematoxylin and rinsed with deionized water. The
113 deparaffinization, pretreatment, primary staining, secondary staining and
114 counterstaining steps were run in a Bond III automated IHC/ISH stainer (Leica,
115 Wetzlar, Germany). Dilutions between 1:20 and 1:500 had been evaluated before
116 selecting 1:40.
117
118 *2.3. Digital image analysis*
119 After sectioning and staining, all glass slides were digitally scanned to the .ndpi file
120 format at ×400, using identical digital scanners at both institutions (Nano Zoomer 2.0
121 HT, Hamamatsu Photonics K.K., Hamamatsu, Japan). The digital image analysis
122 (DIA) software used was the QuPath Bioimage analysis v. 0.2.0 m4 (Bankhead et al.,
123 2017). The software was run on a standard off-the-shelf laptop computer (Apple Inc.
124 Cupertino, CA).
125 For assessment of the level of nBAP-1 expression, one positive cell (red
126 chromogen in nucleus) and one negative cell (haematoxylin but no red chromogen in
127 nucleus) was calibrated in each digitally scanned tissue section. All other parameters
128 were left at default in order to limit time consumption and maintain ease of use.
129 Tumors were then screened under low magnification (40×) and the area exhibiting the
130 most intense nBAP-1 staining selected for grading. Nuclear immunoreactivity was
131 evaluated at 200×, in a circular 0.5 mm-diameter region of interest (corresponding to
132 the field of view in a light microscope with a 400× objective) by automatic
133 classification (positive cell detection). Based on previous publications, the nBAP-1
134 expression was classified as “high” if immunoreactivity was detected in >30 % of

135 tumor cells within the region of interest, and "low" if it was detected in ≤ 30 % of
136 tumor cells (See et al., 2019; Stålhammar et al., 2019; Szalai et al., 2018).
137 A workflow for morphometric analysis was then created, including the
138 following steps for each tumor: A) Identification of all cells within the region of
139 interest, using the software's cell detection function with the following setttings:
140 Background nucleus radius 8 µm, median filter radius 0 µm, sigma 1.5 µm, minimum
141 nucleus area 7.5 μm^2, maximum nucleus area 200 μm^2, threshold 0.1, max
142 background intensity 2 and cell expansion 5 µm. B) Measurement in each detected
143 cell in each region of interest of the following 12 cell morphometric variables: 1)
144 Nucleus area (μm^2). 2) Nucleus perimeter (µm). 3) Nucleus circularity. 4) Nucleus
145 max caliper (µm). 5) Nucleus min caliper (µm). 6) Nucleus eccentricity. 7) Cell area
146 (μm^2). 8) Cell perimeter (µm). 9) Cell circularity. 10) Cell max caliper. 11) Cell min
147 caliper. 12) Nucleus to cell area ratio (figure 1).
148 Tumor areas with intense inflammation, heavy pigmentation, bleeding,
149 necrosis or poor fixation were avoided. nBAP-1 classification and morphometric
150 analysis was performed blinded to all other patient data including outcome. For
151 measurement of interobserver concordance, two human observers performed the
152 digital morphometry (morphometric variable above or below median value) and
153 nBAP-1 classification (high or low) independently and blinded to patient outcomes.
154
155 *2.4. Gene expression classification*
156 Tumor tissue samples were obtained from freshly enucleated eyes by fine needle
157 aspiration. The contents of the needle hub were transferred into one of two RNAse-
158 free cryovials. Using the same needle, extraction buffer from the second cryovial was

159 aspirated and expelled into the first. This was then placed in a specimen bag,
160 immediately frozen to -80° C and shipped on dry ice for gene expression classification
161 based on 12 discriminating genes (*HTR2B, ECM1, RAB31, CDH1, FXR1, LTA4H,*
162 *EIF1B, ID2, ROBO1, LMCD1, SATB1*, and *MTUS1*) and 3 control genes (*MRPS21*,
163 *RBM23*, and *SAP130*) at a commercial laboratory (Castle Biosciences Inc.
164 Friendswood, TX, USA). Expression levels of the gene products are used to
165 categorize tumors as either class 1 with low metastatic risk, or class 2 with high
166 metastatic risk (Onken et al., 2012).
167
168 *2.5. Statistical methods*
169 Differences with a $p<0.05$ were considered significant, all p-values being two-sided.
170 The deviation of all clinicopathological variables from normal distribution was
171 statistically significant, when evaluated by the Shapiro–Wilk test ($p<0.05$). For
172 statistical tests of these variables, we therefore used the Mann-Whitney *U* test, which
173 does not assume normally distributed data. The deviation of all morphometric
174 variables from normal distribution was however not statistically significant ($p>0.05$),
175 why we used Students T-tests for these. For comparisons of categorical variables,
176 two-by-two tables and Fisher's exact test were used. For correlation to Cox
177 Proportional Hazards for metastasis and Kaplan-Meier metastasis-free survival,
178 patients were split into two groups based on 1) the median value of each
179 morphometric variable, and 2) receiver operating characteristics (ROC) in the training
180 cohort, with equal emphasis on sensitivity and specificity for the development of
181 metastasis. The thresholds established in the training cohort were then tested in the
182 validation cohort. In evaluation of interobserver concordance, the percentage of

183 identically classified cases and Cohen's kappa statistics (κ) were computed (Cohen,
184 1960). Metastasis-free follow-up was defined as the time in months from enucleation
185 to the last occasion patients without metastases was seen or in contact alive. All
186 statistical analyses were performed using IBM SPSS statistics version 25 (Armonk,
187 NY, USA).
188
189 **3. Results**
190 *3.1. Descriptive statistics*
191 The mean age at enucleation of patients included in this study was 66 years (SD 15).
192 Of 27 patients, 15 were men and 12 women. 25 tumors originated in the choroid and 2
193 in the ciliary body. The cell type was mixed in 18 patients, spindle in 5 and epitheloid
194 in 4. Mean tumor thickness was 8.6 mm (SD 3.7) and mean diameter 15.8 mm (SD
195 4.8). 12 tumors were of gene expression class 2 and 15 of class 1a or 1b. 14 tumors
196 had low nBAP-1 expression and 13 high. Mean metastasis-free follow-up time was 47
197 months (SD 76, Table 1).
198 The average number of cells analyzed in each tumor was 1957 (SD 349),
199 which took an average of 74 seconds (SD 21) for nBAP-1 classification and 71
200 seconds (SD 17) for morphometric analysis, adding up to 145 seconds or nearly two-
201 and-a-half minutes per tumor.
202
203 *3.2. Interobserver concordance*
204 Identical nBAP-1 classification was obtained for 25 of 27 tumors (93 %), yielding a
205 Cohen's kappa statistic indicating almost perfect agreement (κ=0.85).

206 Identical morphometric classification (morphometric variable above/below
207 median value) was obtained for ≥ 85 % of tumors in all 12 variables, yielding
208 substantial or almost perfect agreement (κ 0.70–0.93, Table 2).
209
210 *3.3. Morphometry versus nBAP-1 expression and gene expression class*
211 The mean nucleus area, nucleus perimeter, nucleus max caliper and nucleus to cell
212 area ratio were significantly greater in tumors with low nBAP-1 expression. Nucleus
213 circularity, nucleus min caliper, nucleus eccentricity and cell area, cell perimeter, cell
214 circularity, cell max and min caliper were however not significantly different (Table
215 3a).
216 Similarly, the mean nucleus area, nucleus perimeter, nucleus max caliper and
217 nucleus to cell area ratio, but not the other morphometric variables, were significantly
218 greater in tumors of gene expression class 2 (Table 3b).
219
220 *3.4. Adjusted thresholds*
221 The 4 morphometric variables that correlated to nBAP-1 and gene expression class
222 were analyzed with ROC, with equal emphasis on sensitivity and specificity for the
223 development of metastasis. Mean nucleus area achieved an area under the curve
224 (AUC) of 0.67 (sensitivity 67 %, specificity 50 %, p=0.40) at threshold 27.5 μm^2;
225 Mean nucleus perimeter achieved an area under the curve (AUC) of 0.73 (sensitivity
226 67 %, specificity 70 %, p=0.24) at threshold 21.5 μm; Mean nucleus max caliper
227 achieved an area under the curve (AUC) of 0.80 (sensitivity 67 %, specificity 90 %,
228 p=0.13) at threshold 8 μm; and mean nucleus to cell area ratio achieved an area under

229 the curve (AUC) of 0.60 (sensitivity 67 %, specificity 50 %, p=0.61) at threshold 0.28
230 (figure 2).
231
232 *3.5. Regression analysis and survival*
233 In univariate Cox proportional hazards analyses of nucleus area, nucleus perimeter,
234 nucleus max caliper and nucleus to cell area ratio, none was an individual predictor of
235 metastasis (Table 4).
236 In Kaplan-Meier analysis, patients had significantly shorter metastasis-free
237 survival if their tumors had low nBAP-1 expression (Log-Rank p=0.002) or gene
238 expression class 2 (Log-Rank p=0.004), but not if they had a mean nucleus area,
239 nucleus perimeter, nucleus max caliper and nucleus to cell area ratio greater than the
240 median (Log-Rank p=0.20–0.83). When using the thresholds established in the
241 training cohort, mean nucleus max caliper > 8 μm was associated with metastasis-free
242 survival (Log-Rank p=0.05), whereas the other ROC-adjusted variables did not
243 separate groups with significant survival differences (Log-rank p=0.18–0.95, figure
244 3).
245
246 **4. Discussion**
247 In this study, we have shown that digital image analysis of uveal melanoma cell
248 morphometry can be fast and highly reproducible, and that variables describing the
249 shape and size of the nuclei correlate to nBAP-1 expression as well as gene
250 expression class. Patients with tumors that had large nuclei, as defined by their max
251 caliper, had significantly worse prognosis. On the other hand, no variable describing
252 the shape and size of the entire tumor cell correlated to the established prognostic

253 factors, indicating that for prognosis, the morphological characteristics of tumor
254 nuclei are more important.

255 The prognostic importance of cell morphology is by no means a novel
256 discovery. However, reproducibility, time consumption and level of expertise
257 required to make reliable assessments of morphometry have limited its utility.
258 Modern user-friendly digital image analysis techniques offer an attractive solution to
259 these problems, and for the first time we can now objectively quantitate morphometry
260 parameters in thousands of cells at a time.

261 In turn, changes to the size and shape of tumor cells are but a consequence of
262 changes in the genotype. As found by Onken *et al*. the helix-loop-helix inhibitor *ID2*
263 suppress the epithelial phenotype associated with an enlarged nucleus (Onken et al.,
264 2006). Loss of *ID2* up-regulates the epithelial adhesion molecule E-cadherin, which in
265 turn promotes the anchorage-independent cell growth required for metastasis.
266 Consequently, we regard the morphometric characteristics investigated here as
267 biomarkers of the state of the genotype.

268 Limitations of this study include a small sample size. Inclusion of a larger
269 number of patients may have revealed additional significant differences. This was
270 however prevented, primarily by the lack of tumors in our archives for which gene
271 expression classification was available. Far-reaching conclusions from our survival
272 analysis are thereby precluded. Substantial investments in digital scanning capacity is
273 required before the method presented here can be used. The time consumption
274 specified will most likely be longer for users without general experience in the
275 operation of home computers, and does not include preanalytical operations such as
276 digital scanning and loading and unloading of glass slides. Last, our sample is not

representative of all patients with uveal melanoma. We have only investigated the feasibility of digital morphometry in enucleated specimens without previous plaque brachytherapy. A large proportion of patients with uveal melanoma undergo primary plaque brachytherapy or proton beam radiotherapy, and may never require enucleation. It remains unclear if the digital morphometry characteristics of small uveal melanomas is different from the relatively large tumors investigated here. Accordingly, we encourage future studies to confirm these results in larger cohorts that includes smaller tumors .

Funding

This work was supported in part by Cancerfonden, Karolinska Institutet (Karolinska Institutets stiftelsemedel för ögonforskning) and Stockholm County Council (Stockholms läns landsting).

References

Arnljots, T.S., Al-Sharbaty, Z., Lardner, E., All-Eriksson, C., Seregard, S., Stålhammar, G., 2018. Tumour thickness, diameter, area or volume? The prognostic significance of conventional versus digital image analysis-based size estimation methods in uveal melanoma. Acta Ophthalmol 96, 510-518.

Augsburger, J.J., Corrêa, Z.M., Shaikh, A.H., 2009. Effectiveness of Treatments for Metastatic Uveal Melanoma. American Journal of Ophthalmology 148, 119-127.

Bankhead, P., Loughrey, M., Fernández, J., Dombrowski, Y., McArt, D., Dunne, P., McQuaid, S., Gray, R., Murray, L., Coleman, H., James, J., Salto-Tellez, M., Hamilton, P., 2017. QuPath: Open source software for digital pathology image analysis. Sci Rep 7, 16878-16878.

Bornfeld, N., Prescher, G., Becher, R., Hirche, H., Jöckel, K.H., Horsthemke, B., 1996. Prognostic implications of monosomy 3 in uveal melanoma. The Lancet 347, 1222-1225.

Callender, G., 1931. Malignant Melanotic tumors of the eye. A study of histologic types in 111 cases. Trans. Am. Acad. Ophthalmol. Otolaryngol. 36, 131-142.

Carvajal, R.D., Schwartz, G.K., Tezel, T., Marr, B., Francis, J.H., Nathan, P.D., 2016. Metastatic disease from uveal melanoma: treatment options and future prospects. British Journal of Ophthalmology.

Cohen, J., 1960. A Coefficient of Agreement for Nominal Scales. Educational and Psychological Measurement 20, 37-46.

Coleman, K., Baak, J.P.A., van Diest, P.J., Mullaney, J., 1996. Prognostic Value of Morphometric Features and the Callender Classification in Uveal Melanomas. Ophthalmology 103, 1634-1641.

Gamel, J.W., McCurdy, J.B., McLean, I.W., 1992. A comparison of prognostic covariates for uveal melanoma. Investigative ophthalmology & visual science 33, 1919.

Gamel, J.W., McLean, I.W., Greenberg, R.A., Zimmerman, L.E., Lichtenstein, S.J., 1982. Computerized histologic assessment of malignant potential: A method for determining the prognosis of uveal melanomas. Human Pathology 13, 893-897.

Guyon, I., 1997. A scaling law for the validation-set training-set size ratio. At&t Bell Laboratories, Berkeley California, pp. 1-11.

Kivelä, T., Simpson, E.R., Grossniklaus, H.E., Jager, M.J., Singh, A.D., Caminal, J.M., Pavlick, A.C., Kujala, E., Coupland, S.E., Finger, P.T., 2017. Uveal Melanoma, AJCC Cancer Staging Manual, 8 ed. Springer, Chicago, pp. 805-817.

Kujala, E., Mäkitie, T., Kivelä, T., 2003. Very long-term prognosis of patients with malignant uveal melanoma. Invest Ophthalmol Vis Sci 44, 4651-4659.

McLean, I., Foster, W., Zimmerman, L., Gamel, J., 1983. Modifications of Callender's classification of uveal melanoma at the Armed Forces Institute of Pathology. Am J Ophthalmol 96, 502-509.

Onken, M.D., Ehlers, J.P., Worley, L.A., Makita, J., Yokota, Y., Harbour, J.W., 2006. Functional gene expression analysis uncovers phenotypic switch in aggressive uveal melanomas. Cancer research 66, 4602.

Onken, M.D., Worley, L.A., Char, D.H., Augsburger, J.J., Correa, Z.M., Nudleman, E., Aaberg, T.M., Altaweel, M.M., Bardenstein, D.S., Finger, P.T., Gallie, B.L., Harocopos, G.J., Hovland, P.G., McGowan, H.D., Milman, T., Mruthyunjaya, P., Simpson, E.R., Smith, M.E., Wilson, D.J., Wirostko, W.J., Harbour, J.W., 2012. Collaborative Ocular Oncology Group report number 1: prospective validation of a multi-gene prognostic assay in uveal melanoma. Ophthalmology 119, 1596-1603.

Seddon, J.M., Polivogianis, L., Hsieh, C.-C., Albert, D.M., Gamel, J.W., Gragoudas, E.S., 1987. Death From Uveal Melanoma: Number of Epithelioid Cells and Inverse SD of Nucleolar Area as Prognostic Factors. Archives of Ophthalmology 105, 801-806.

See, T.R.O., Stålhammar, G., Phillips, S.S., Grossniklaus, H.E., 2019. BAP1 Immunoreactivity Correlates with Gene Expression Class in Uveal Melanoma. Ocular Oncology and Pathology, 1-9.

Shields, C.L., Furuta, M., Thangappan, A., Nagori, S., Mashayekhi, A., Lally, D.R., Kelly, C.C., Rudich, D.S., Nagori, A.V., Wakade, O.A., Mehta, S., Forte, L., Long, A., Dellacava, E.F., Kaplan, B., Shields, J.A., 2009. Metastasis of Uveal Melanoma Millimeter-by-Millimeter in 8033 Consecutive Eyes. Archives of Ophthalmology 127, 989-998.

Singh, N., Bergman, L., Seregard, S., Singh, A.D., 2014. Epidemiologic Aspects, in: Damato, B., Singh, A.D. (Eds.), Clinical Ophthalmic oncology: Uveal tumors, 2 ed. Springer, Berlin, Heidelberg, pp. 75-87.

Stålhammar, G., Fuentes Martinez, N., Lippert, M., Tobin, N.P., Mølholm, I., Kis, L., Rosin, G., Rantalainen, M., Pedersen, L., Bergh, J., Grunkin, M., Hartman, J., 2016. Digital image analysis outperforms manual biomarker assessment in breast cancer. Modern pathology : an official journal of the United States and Canadian Academy of Pathology, Inc 29, 318.

Stålhammar, G., Robertson, S., Wedlund, L., Lippert, M., Rantalainen, M., Bergh, J., Hartman, J., 2018. Digital image analysis of Ki67 in hot spots is superior to both manual Ki67 and mitotic counts in breast cancer. Histopathology 72, 974-989.

Stålhammar, G., See, T.R.O., Phillips, S., Seregard, S., Grossniklaus, H.E., 2019. Digital Image Analysis of BAP-1 Accurately Predicts Uveal Melanoma Metastasis. Translational vision science & technology 8, 11.

Szalai, E., Wells, J.R., Ward, L., Grossniklaus, H.E., 2018. Uveal Melanoma Nuclear BRCA1-Associated Protein-1 Immunoreactivity Is an Indicator of Metastasis. Ophthalmology 125, 203-209.

Legends

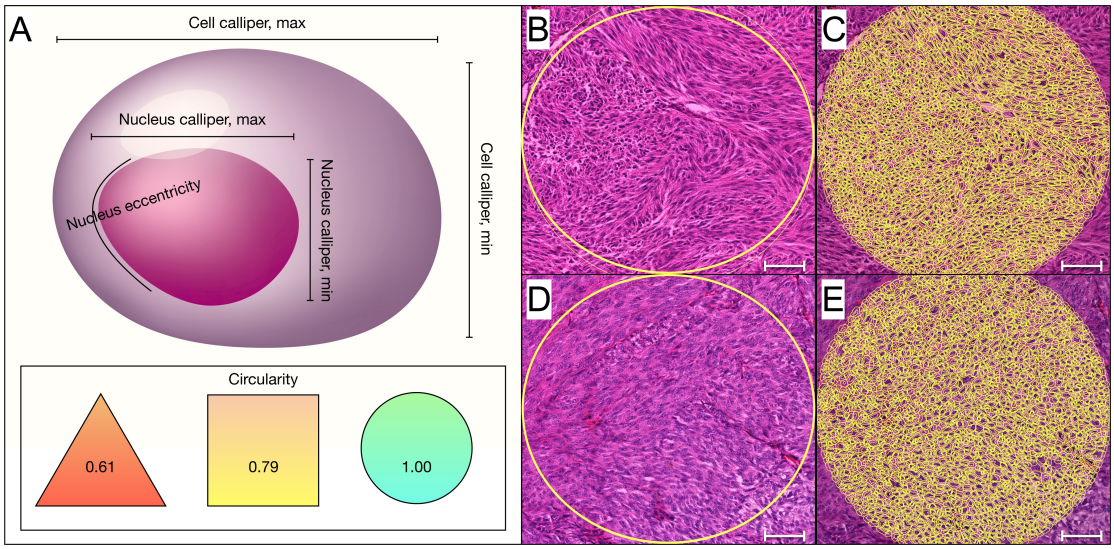

Figure 1. Illustration of cell morphometric measurements. A) Calipers denotes the largest and smallest diameters of the nucleus and cell. Nucleus eccentricity is a measure of how much the nucleus deviates from a spherical shape, presented as a number between 0.00 and 1.00. A completely spherical nucleus have an eccentricity of 0.00, a nucleus with the shape of an elliptical 3D solid would have an eccentricity

380 of 0.5, whereas a 3D conical distribution would have a value of 1.00. Circularity
381 compares the perimeter of a shape to the area it contains, and is calculated by four
382 times π times the area divided by the perimeter squared. The circularity of a circle is
383 1.00, and less for less circular objects. B) A circular 0.5 mm-diameter region of
384 interest (corresponding to the field of view in a light microscope with a 400×
385 objective) was defined in each tumor. Within this region of interest, each cell was
386 analyzed for nBAP-1 expression and 12 morphometric variables describing the size
387 and shape of cells and nuclei. C) The morphometric variables have been automatically
388 identified within the region of interest shown in B. D and E) In another tumor, cells
389 have slightly larger, more rounded nuclei with prominent nucleoli, corresponding to
390 what would be known as epitheloid cells. Cell illustration by iStock.com/Vitalii
391 Dumma, East Ukraine Volodymyr Dahl National University Scale bars: 100 μm..
392

***n* =**	27
Mean age at diagnosis, years (SD)	66 (15)
Sex, n (%)	
Female	15 (56)
Male	12 (44)
Primary tumor location, n (%)	
Choroid	25 (93)
Ciliary body	2 (7)
Iris	0 (0)
Cell type, n (%)	
Spindle	5 (19)
Epitheloid	4 (15)
Mixed	18 (67)
Mean tumor thickness, mm (SD)	8.6 (3.7)

Mean tumor diameter, mm (SD)	15.8 (4.8)
Previous brachytherapy or TTT, n (%)	
No	27 (100)
Yes	0 (0)
AJCC T-category, n (%)	
1	0 (0)
2	7 (26)
3	14 (52)
4	6 (22)
Gene expression class, n (%)	
1a	9 (33)
1b	6 (22)
2	12 (44)
DIA nBAP-1 classification, n (%)	
High	13 (48)
Low	14 (52)
Follow-up months, mean (SD)[§]	47 (76)

Table 1. Characteristics of patients and tumors included in this study. SD, standard deviation. TTT, Transpupillary thermotherapy.

	Interobserver concordance (%)	**Cohen's κ**
Nucleus area	85	0.70
Nucleus perimeter	85	0.70
Nucleus circularity	96	0.93
Nucleus caliper, max	85	0.70
Nucleus caliper, min	89	0.78
Nucleus eccentricity	96	0.93
Cell area	85	0.70
Cell perimeter	85	0.70
Cell circularity	93	0.85
Cell caliper, max	85	0.70

Cell caliper, min	85	0.70
Nucleus to cell area ratio	96	0.93

396 Table 2. Interobserver concordance and Cohen's kappa statistics in classification of

397 each morphometric variable as above or below the median value.

398

	nBAP-1 high (n=13)	**nBAP-1 low (n=14)**	***P***
Nucleus area, μm^2 (SD)	24.31 (4.38)	28.34 (3.40)	0.013
Nucleus perimeter, µm (SD)	19.61 (1.78)	21.37 (1.28)	0.0066
Nucleus circularity	0.76 (0.04)	0.75 (0.04)	0.41
Nucleus caliper, max µm (SD)	7.52 (0.65)	8.21 (0.58)	0.0074
Nucleus caliper, min µm (SD)	4.43 (0.59)	4.67 (0.36)	0.20
Nucleus eccentricity (SD)	0.76 (0.03)	0.77 (0.04)	0.52
Cell area, μm^2 (SD)	88.50 (15.10)	94.58 (12.42)	0.26
Cell perimeter, µm (SD)	37.05 (3.26)	38.33 (2.53)	0.26
Cell circularity	0.77 (0.01)	0.77 (0.01)	0.70
Cell caliper, µm (SD)	13.62 (1.22)	14.09 (0.97)	0.27
Cell caliper, µm (SD)	9.00 (0.79)	9.29 (0.59)	0.30
Nucleus to cell area ratio	0.28 (0.03)	0.30 (0.02)	0.031

399 Table 3a.

400 Average values and Students T-tests of cell morphometric variables in tumors of high

401 versus low nBAP-1 expression. SD, standard deviation.

402

	Gene expression class 1a or 1b (n=15)	**Gene expression class 2 (n=12)**	***P***
Nucleus area, μm^2 (SD)	24.89 (4.40)	28.28 (3.59)	0.041
Nucleus perimeter, µm (SD)	19.84 (1.76)	21.37 (1.39)	0.0022
Nucleus circularity	0.76 (0.04)	0.75 (0.04)	0.42

Nucleus caliper, max µm (SD)	7.59 (0.63)	8.23 (0.63)	0.016
Nucleus caliper, min µm (SD)	4.48 (0.57)	4.65 (0.37)	0.39
Nucleus eccentricity (SD)	0.76 (0.03)	0.77 (0.04)	0.33
Cell area, μm^2 (SD)	89.90 (14.59)	93.83 (13.16)	0.48
Cell perimeter, µm (SD)	37.34 (3.13)	38.18 (2.70)	0.47
Cell circularity	0.77 (0.01)	0.77 (0.01)	0.64
Cell caliper, max µm (SD)	13.71 (1.15)	14.06 (1.05)	0.42
Cell caliper, min µm (SD)	9.23 (0.61)	9.23 (0.61)	0.62
Nucleus to cell area ratio	0.28 (0.03)	0.30 (0.02)	0.024

Table 3b.

Average values and Students T-tests of cell morphometric variables in tumors of gene expression class 1a or 1b versus 2. SD, standard deviation.

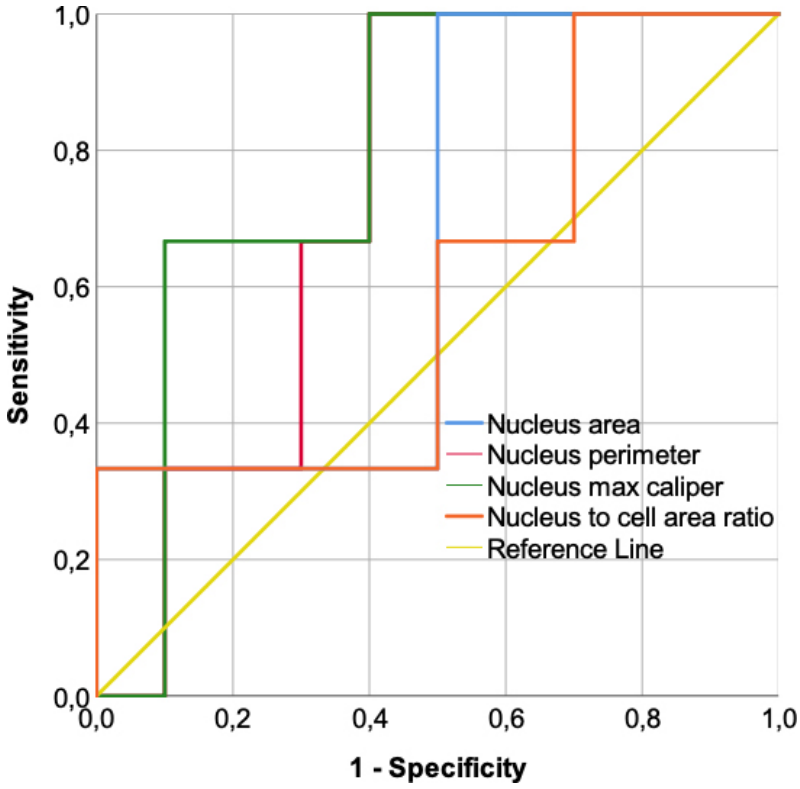

Figure 2.

408 Receiver operating characteristics (ROC) of the mean nucleus area, nucleus
409 perimeter, nucleus max caliper and nucleus to cell area ratio in the training cohort
410 (*n*=13), with equal emphasis on sensitivity and specificity for the development of
411 metastasis. Mean nucleus area (blue line) achieved an area under the curve (AUC) of
412 0.67 (sensitivity 67 %, specificity 50 %, p=0.40) at threshold 27.5 μm^2; Mean nucleus
413 perimeter (pink line) achieved an area under the curve (AUC) of 0.73 (sensitivity 67
414 %, specificity 70 %, p=0.24) at threshold 21.5 μm; Mean nucleus max caliper (green
415 line) achieved an area under the curve (AUC) of 0.80 (sensitivity 67 %, specificity 90
416 %, p=0.13) at threshold 8 μm; and mean nucleus to cell area ratio (orange line)
417 achieved an area under the curve (AUC) of 0.60 (sensitivity 67 %, specificity 50 %,
418 p=0.61) at threshold 0.28.
419

	Regression coefficient, β (SE)	**Wald statistic**	***P***	**Hazard coefficient, Exp(b) (95 % CI)**
Univariate Cox proportional hazards				
Nucleus area ≥ median	0.2 (0.7)	0.05	0.83	1.17 (0.3–4.8)
Nucleus perimeter ≥ median	0.9 (0.7)	1.5	0.22	2.5 (0.6–10.4)
Nucleus caliper, max ≥ median	0.9 (0.7)	1.5	0.22	2.5 (0.6–10.4)
Nucleus to cell area ratio ≥ median	0.4 (0.7)	0.4	0.52	1.6 (0.4–5.9)

420 Table 4.
421 Cox Proportional Hazards analysis of the association between metastasis-free survival
422 and cell morphometric variables. No method was individually associated with
423 shortened metastasis-free survival.
424 SE, standard error.
425

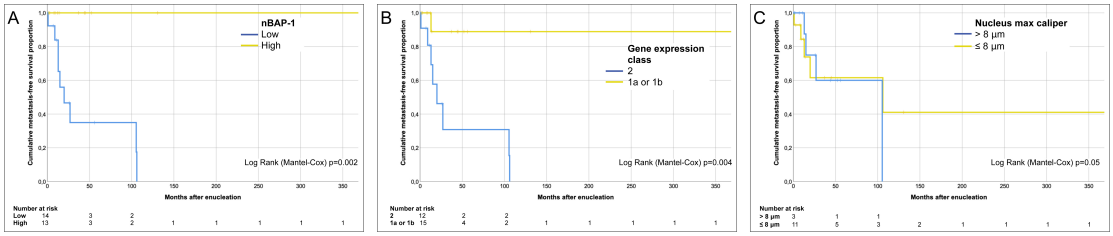

Figure 3.

Kaplan-Meier curves, cumulative metastasis-free survival. A) Patients with tumors with high nBAP-1 expression (yellow) versus low (blue), as defined by digital image analysis using a mean of <30 % stained tumor nuclei as cutoff (Log-Rank p=0.002). B) Patients with tumors of gene expression class 1a or 1b (yellow) versus 2 (blue, Log-Rank p=0.004). C) Patients in the validation cohort (*n*=14) with mean nucleus max caliper ≤ 8 µm (yellow) versus > 8 µm (blue), which was the threshold established in the training cohort (Log-Rank p=0.05).

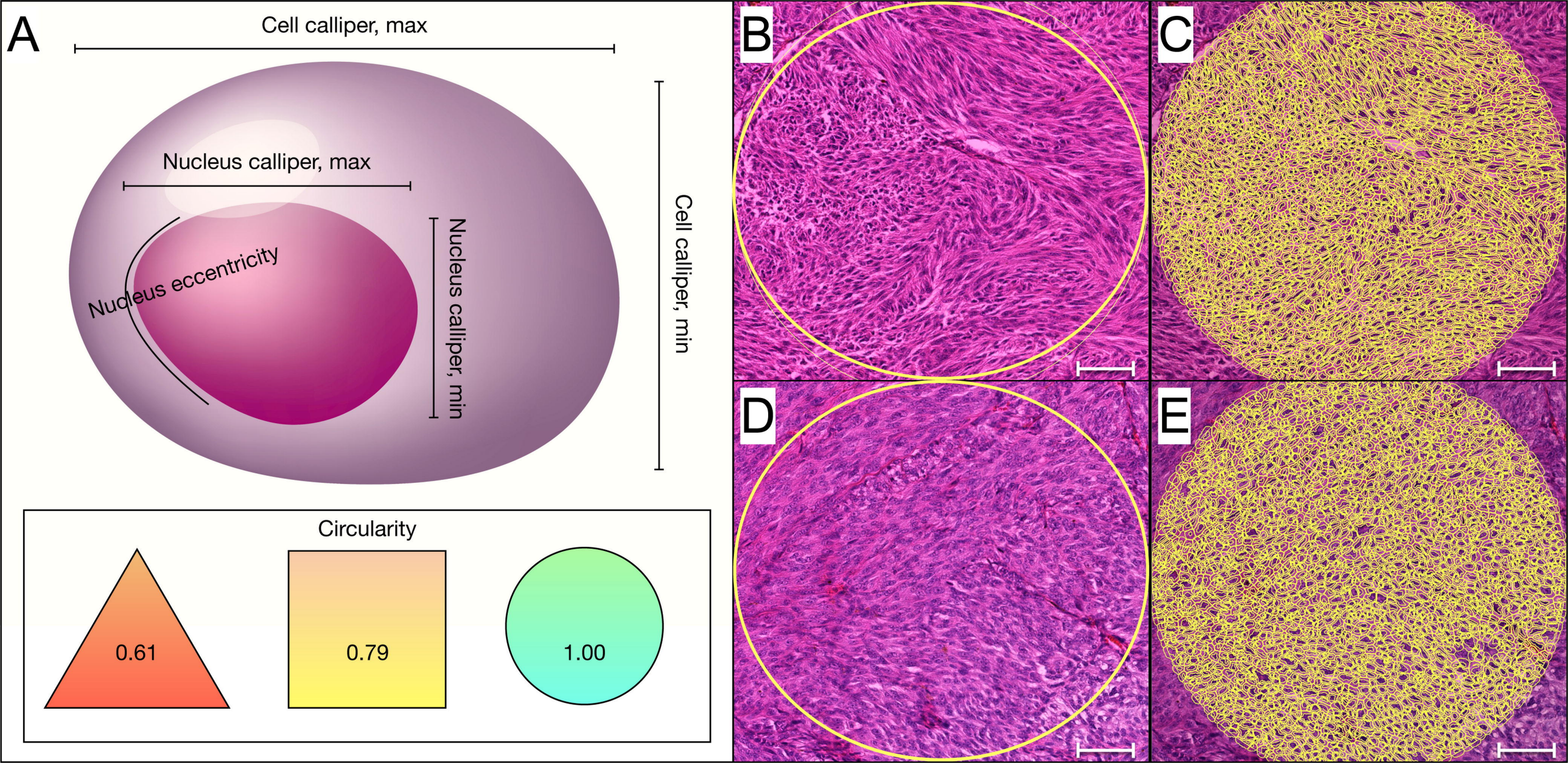
A
Cell calliper, max
Nucleus calliper, max
Nucleus eccentricity
Nucleus calliper, min
Cell calliper, min
Circularity
0.61
0.79
1.00
B
C
D
E

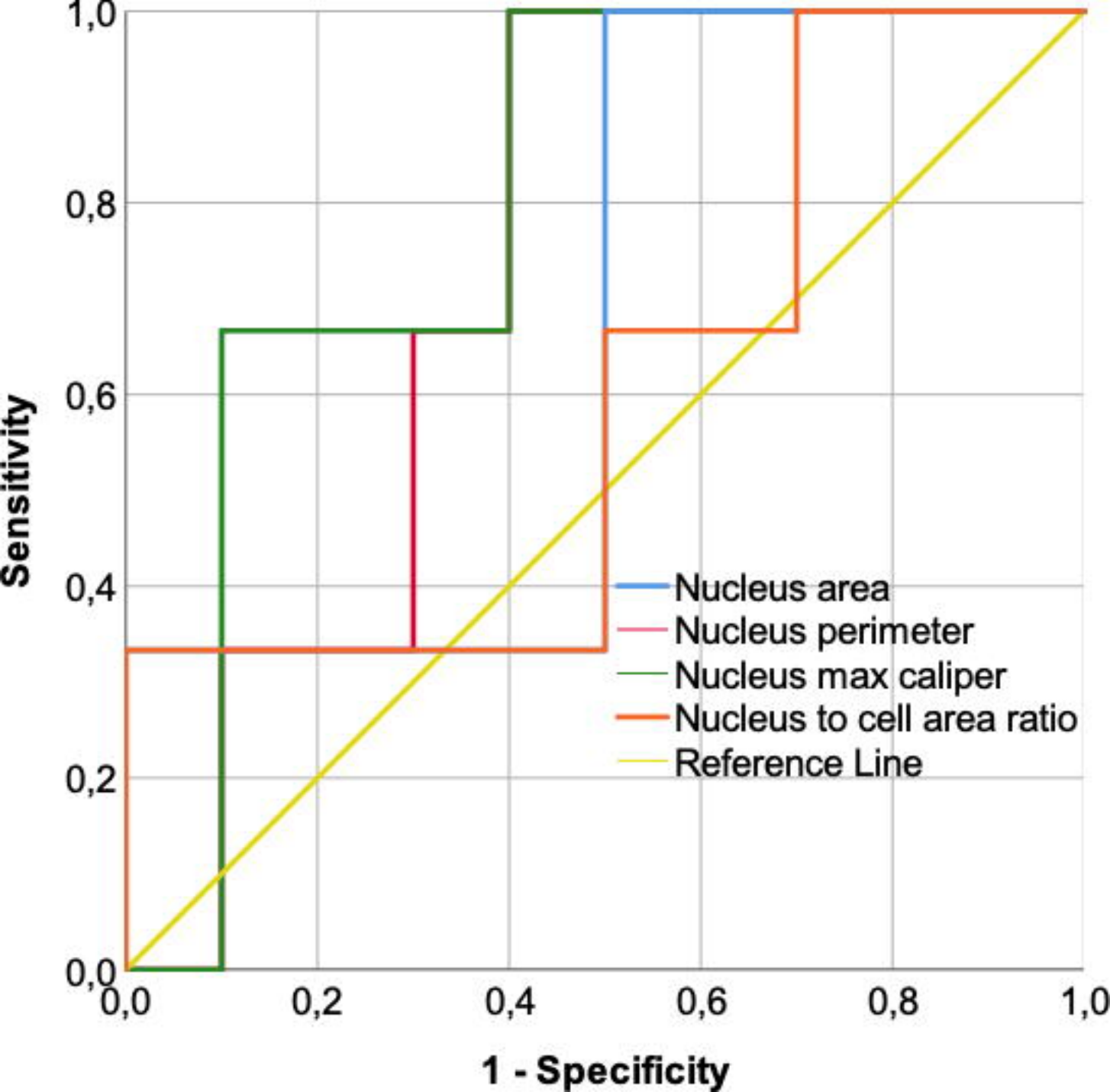
1,0
0,8
0,6
0,4
0,2
0,0
Sensitivity
0,0
0,2
0,4
0,6
0,8
1,0
1 - Specificity
Nucleus area
Nucleus perimeter
Nucleus max caliper
Nucleus to cell area ratio
Reference Line

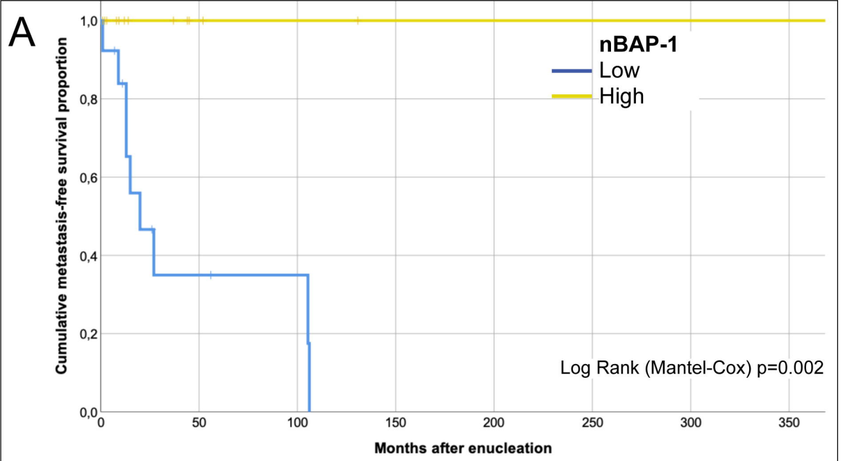
A
nBAP-1
Low
High
Cumulative metastasis-free survival proportion
1,0
0,8
0,6
0,4
0,2
0,0
0
50
100
150
200
250
300
350
Months after enucleation
Log Rank (Mantel-Cox) p=0.002
Number at risk
Low 14 3 2
High 13 3 2 1 1 1 1 1

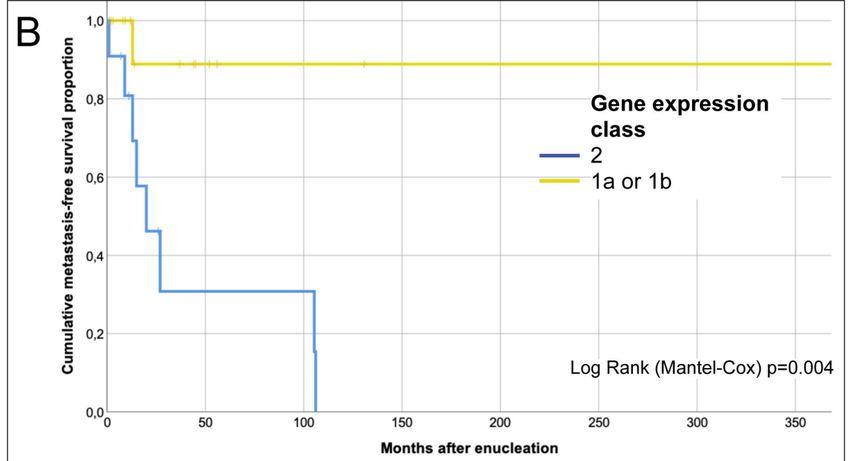
B
Gene expression class
2
1a or 1b
Cumulative metastasis-free survival proportion
1,0
0,8
0,6
0,4
0,2
0,0
0
50
100
150
200
250
300
350
Months after enucleation
Log Rank (Mantel-Cox) p=0.004
Number at risk
2 12 2 2
1a or 1b 15 4 2 1 1 1 1 1

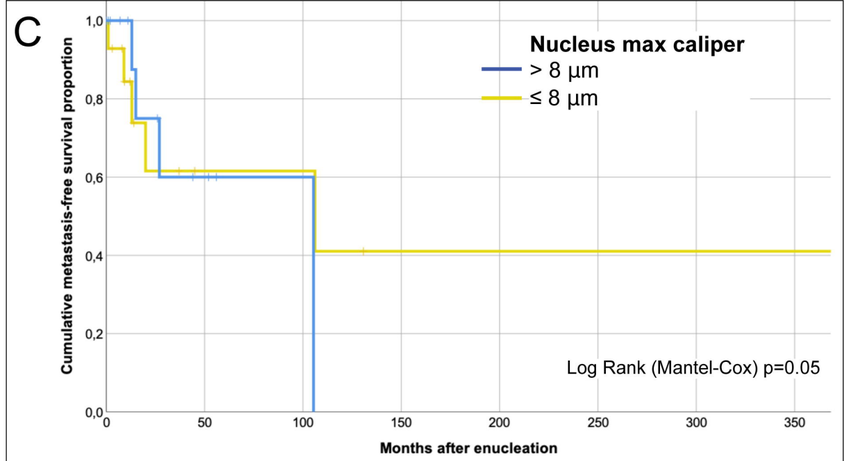
C
Nucleus max caliper
> 8 µm
≤ 8 µm
Cumulative metastasis-free survival proportion
1,0
0,8
0,6
0,4
0,2
0,0
0
50
100
150
200
250
300
350
Months after enucleation
Log Rank (Mantel-Cox) p=0.05
Number at risk
> 8 µm 3 1 1
≤ 8 µm 11 5 3 2 1 1 1 1